Dalton Transactions

Accepted Manuscript

ROYAL SOCIETY OF CHEMISTRY

www.rsc.org/dalton

Structural and magnetic properties of mixed Co-Ln (Ln = Nd, Sm, Eu, Gd and Ho) diethyleneglycolate complexes

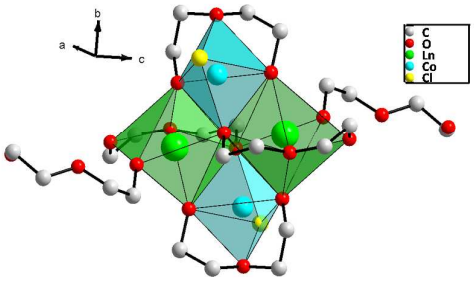

Co-Ln diethyleneglycolates were produced in diethyleneglcol ($degH_2$). They consist of 1D-chains of $[(Ln_2Co_2)(Cl)_2(deg)_4]$ tetramers, in which five- and seven-coordinated Co(II) and Ln(III) cations are antiferromagnetically weakly interacting.

Dalton Transaction

ARTICLE

Structural and magnetic properties of mixed Co-Ln (Ln = Nd, Sm, Eu, Gd and Ho) diethyleneglycolate complexes

Received 00th June 2015,
Accepted 00th January 20xx

DOI: 10.1039/x0xx00000x

www.rsc.org/

A. Abdallah,[a,b,c] T. Gaudisson,[a] R. Sibille,[b] S. Nowak,[a] W. Cheikhrouhou-Koubaa,[c] K. Shinoda,[b] F. François[b] and S. Ammar[a,] †

New hybrid compounds $LnCoCl(deg)_2$ (deg = diethylenglycolate ; Ln = Nd, Sm, Eu, Gd and Ho) have been synthesized by mixing cobalt and rare earth cations in a boiling diethylenegycol ($degH_2$) medium. Their crystallographic structures have been ab initio solved from synchrotron powder diffraction data. They consist of edge sharing tetrameric sub-units $[(Ln_2Co_2)(deg)_4(Cl)_2]$ forming 1D infinite chains along the c parameter of a monoclinic unit cell (SG = C2/c). The five- and seven-coordination of Co^{2+} and Ln^{3+} cations inferred from crystallographic results is confirmed by UV-visible absorption and Extended X-ray Absorption Fine Structure (EXAFS) spectroscopies. In the $LnCoCl(deg)_2$ (Ln = Nd, Sm, ,Eu, Gd, Ho) series, weak antiferromagnetic superexchange interactions have been evidenced, between high spin Co^{2+} and Ln^{3+} orbitally degenerated cations. These materials are considered as potential precursors for the simultaneous reduction of Co-Ln-glycolate species into bimettallic nanoparticles by the polyol process.

Introduction

The investigation of lanthanide (Ln) - transition metal (TM) alloys has been the subject of many fundamental as well as technological studies. They show remarkable intrinsic magnetic properties. Some of them, particularly those crystallizing in the hexagonal $CaCu_5$ structure, are distinguished by large magnetocrystalline anisotropy, high magnetization and high Curie temperature, making them particularly valuable for permanent magnet application. [1-3] Others, mainly amorphous soft ferromagnets with tailorable composition and special atomic structure offer unique magnetocaloric properties thanks to their low eddy current and hysteresis losses, improved corrosion resistance, large specific surface and tunable temperature transition, which are particularly useful for cryogenic magnetic refrigeration in a large operating temperature range. [4] Certain Ln-TM ferrimagnets can exhibit a magnetization compensation temperature TM where the magnetizations of the Ln and TM sublattices cancel each other and similarly an angular compensation temperature TA where the net angular momentum of the two sublattices converge to zero. [5] These properties are intensively regarded for thermo-magnetic writing/reading application. [6] Clearly, TM-Ln alloys show superior bulk magnetic properties and their nanometer-scaled counterparts should do the same compared to TM-TM or Ln-Ln ones. Unfortunately, challenges in controlling the structure, microstructure and phase purity have limited the research on nanoparticles of these compounds.

Nowadays, these alloys are mainly produced by metallurgical methods involving high temperature treatments, higher than 1000°C. Within these methodologies the control of the particle sizes is mostly achieved by mechanical milling which causes considerable material degradation and consequently magnetic properties changes. [7] Progressively, physical techniques, operating around 800°C, were developed to directly produce TM-Ln nano-alloys. Well-ordered crystalline YCo_5 and Y_2Co_{17} nanoparticles were thus successfully synthesized using a plasma-condensation-type cluster-deposition method, where atomic metal vapors of Y and Co were produced from Y-Co bulk composite. [8] Wet-chemical routes, operating between 200 and 300°C, were also developed to tentatively prepare TM-Ln nanoparticles. The first one consists of a thermal decomposition of two distinguished TM and Ln organometallic precursors. Unfortunately, due to the highly negative redox potential of Ln compared to that of TM cations, the simultaneous reduction was not possible and segregated particles with a TM metal core surrounded by a Ln oxide shell were produced, requiring a subsequent reductive annealing at a temperature comprised between 400 and 800°C to obtain the desired metallic objects, with a poor chemical composition and structural control. [9,10] The second way is usually called the polyol process and it consists of the reduction of dissolved metal salts in a polyol medium, offering compared to the previous ones, large-scale synthesis without major economical constraints. [11] Indeed, the polyol acts as a solvent for the metal salts, and as a reducing agent and growth medium for the metal particles. Several TM and TM-TM nanoparticles were already prepared in polyol with controlled morphology. [12] Recently, it was applied to the production of TM-Ln nanoparticles, mainly Co-Sm ones. Matsushita at al. [13] succeeded to

[a] ITODYS, Université Paris Diderot, Sorbonne Paris Cité, CNRS UMR-7086, rue Jean-Antoine de Baïf, F-75205 Paris France.
[b] Institut Jean Lamour, Université de Lorraine, CNRS UMR-7198, Parc de Saurupt, F-54011 Nancy France.
[c] LPM, Faculté des Sciences de Sfax, Université de Sfax, Tu-3000 Sfax, Tunisia.
[d] IMRAM, Tohoku University, 1-1 Katahira 2-chome, Aoba-ku, J-980-8577 Sendai Japan.
† Corresponding author: ammarmer@univ-paris-diderot.fr
Electronic Supplementary Information (ESI) available: See DOI: 10.1039/x0xx00000

prepare directly $SmCo_x$ nanoparticles, by dissolving carboxylate Co and Sm salts in a polyol solvent (under basic conditions) and by adding in the reaction medium a small amount of Au salt. They reported that otherwise the Sm^{3+} ions are not reduced pointing out the catalytic role of the in situ formed Au nanoparticles. Despite these very encouraging results, they didn't succeed to control the chemical composition of the produced nano-alloys and reported a systematic large samarium content deficiency. Chinasamy et al. [14] replaced carboxylates by nitrates and produced magnetic black powder and based only on its X-ray diffraction (XRD) analysis, they claimed that they succeeded to produce $SmCo_5$ phase. In fact, they yielded to cobalt carbides; the XRD patterns of Co_2C and $SmCo_5$ are similar and make the confusion possible. [15]

The co-reduction of Ln and TM cations using the polyol process remains questionable and the optimization of the experimental parameters is still required. To the best of our knowledge, the formation of metal nanoparticles in liquid polyols is preceded by the dissolution of the precursor salts, generally carboxylates, and their solvation. In certain cases, the *in situ* formed complexes interact to each other and form solid intermediate phases, mainly polymeric glycolates, [16] which act as metal cation reservoirs, whom dissolution, under basic condition, control the kinetic of metal particles nucleation and growth. [17] The reduction occurs on the in situ formed (by a direct ligand exchange) glycolate complexes or on those liberated by the subsequent dissolution of the solid intermediate phase. It proceeds through the progressive conversion of soluble M^{II}-glycolate species to M^0 utilizing very probably the electrons from the nearest carbon center of the attached glycolate ligand to form a double bond with the oxygen atom. [18] In this context, the material processing approach which consists of, first, producing in polyol, an intermediate solid phase, in which both TM and Ln cations are coordinated, ideally to a same glycolate bridging ligand, within the desired atomic ratio, and, second, using it as a starting material for the simultaneous reduction of these cations should be tried. Indeed, if this could be achieved it should promote alloyed nanoparticles with controlled chemical composition, structure and microstructure.

As a preliminary study, we report in this paper the chemical preparation and structural determination of TM-Ln glycolate complexes, namely Cobalt (II) and Ln (III) (Ln = Nd, Sm, Eu, Gd and Ho) ones, with a special emphasis on how these cations are coordinated to the polyol molecules and how the resulting polyhedra are organized relative to each other. The structural properties of the obtained compounds were determined ab initio from synchrotron powder data. X-ray and UV-Visible absorption spectroscopies were jointly used to confirm with local probes the inferred structure. Their chemical composition was checked by coupling X-ray fluorescence spectrometry (XRF), Fourier Transform Infrared Spectroscopy (FTIR) and thermogravimetry analysis (TGA). Finally, magnetic measurement consisting of the thermal variation of the magnetic susceptibility and the magnetic heat capacity were carried out as a complementary tool in their structure elucidation.

Experimental

General information

All chemicals and solvents were obtained and used directly from the commercial sources. Cobalt (II) acetate, Lanthanide (III) chloride salts were purchased from Sigma-Aldrich. Diethyleneglycol solvent was purchased from Acros Organics (abbreviated here after as $degH_2$ and deg in its fully deprotonated form). Typically, Co and Ln salts (1.2 mmol each) were dissolved in $degH_2$ (50 mL), in the 1:1 atomic ratio. We also introduced in the reaction medium sodium chloride salt (3.6 mmol). Without halogenide anions in the reaction medium, it becomes impossible to form mixed glycolates. The synthesis was performed first with Europium, and then extended to Neodymium, Samarium, Gadolinium and Holmium. The mixture was then heated up to 245°C (6°C/min) and maintained under reflux for 20 min while mechanically stirred. The solution colour turned from blue to purple and a purple powder was then recovered, after cooling down to room temperature, by centrifugation. Washed several time with ethanol, the final powder was dried under vacuum and then stored in a fridge. Elemental analysis of all the produced powders was carried out by X-ray fluorescence spectrometry (XFR). The as-produced powders were first dispersed in water by ultrasonication. 20 µL were then deposited on a clean polycarbonate membrane and analyzed by using certified solutions with appropriate Cl, Co and Ln compositions on an Epsilon 3XL (Panalytical) XRF spectrometer equipped with a silver X-ray tube operating at 20 kV and 750 µA current emissions, during 20s, using an Al-filter (thickness: 20 µm) and under He atmosphere. The collected XRF signal intensities were compared to those of each standard. To complete these analyses, thermogravimetry (TGA) was conducted on all the fresh powders to determine their molecular weight. A Setaram TGDTA-92 thermobalance was used, heating the samples from 20 to 1000 °C (5 °C/min) under different atmospheres, including oxidative (air), inert (N_2) and reductive (N_2-10%H2) ones. Only those performed in air were discussed. Finally, FTIR spectra were recorded on a Bruker Equinos spectrometer in the region 500–4000 cm^{-1} using KBr technique.

Structure determination

The X-ray Diffraction (XRD) patterns of the produced purple powders were first recorded on a D8 Bruker laboratory diffractometer (λ_{Co} = 1.7889 Å) and plotted in Figure 1.

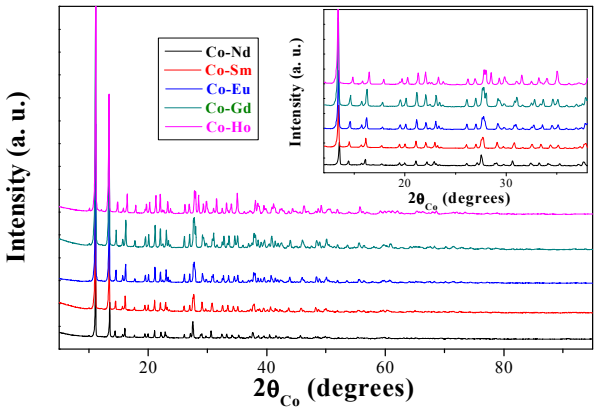

Figure 1. XRD patterns of the produced CoLn-based complexes (Ln = Nd, Sm, Eu, Gd and Ho) recorded on lab diffractometer. A zoom is given for the 15-40° 2θ range, cutting-off the most intense peak in order to better see the less intense ones.

They presented a large amount of well-defined peaks suggesting a high crystalline quality and a low symmetry unit cell but didn't correspond with any tabulated Co and/or Ln based inorganic compounds in ICDD base. Replacing Eu by another Ln cation leads to similar XRD patterns (see the zoom in the inset of Figure 1).

High-resolution XRPD data were then collected at ambient temperature using synchrotron radiation at SOLEIL facilities (Saint Aubin, France) on CRISTAL beamline on the Eu-based compound. A monochromatic beam was extracted from the U20 undulator beam by means of a Si111 double Bragg mirror. Its wavelength (λ = 0.666332 Å) was refined from the powder diagram of the LaB_6 standard (NIST Standard Reference Material 660a), recorded just before the experiment. The high angular resolution is obtained using a two circles diffractometer (SMP–Lyon) equipped with a 21 perfect crystals Si (111) multi-analyzer. The sample enclosed in a capillary (Φ = 0.8 mm) is mounted on a spinner rotating at about 5-10 Hz to improve powder averaging. Patterns were recorded for two hours in the angular range 3.1 < 2θ < 36° with an interval of 0.002°. An initial structural model was found by direct-space methods using FOX program. [19] The initial model was found with the following scatters in the unit cell: two glycolate molecules named 'deg_A' and 'deg_B' each defined as a relaxed 'rigid body' whose orientation and position are free (see Figure S1 in the supporting information section), one europium Eu1, one cobalt Co1 and one chloride Cl1 site. The global optimization procedure was using the parallel tempering algorithm. Rietveld refinements were then performed to reach the final structure of the studied powders. Typically, a pseudo-Voigt function was used for modelling the peak profils (Function 5 in Fullprof [20]). The glycolate relaxed molecules 'deg_A' and 'deg_B' were treated as rigid body during the refinements. A total of 42 parameters were finally refined, including the scale factor, the zero shift, 9 peak profile parameters and 31 intensity dependent parameters: 9 atomic coordinates for Eu, Co and Cl, 3 positional parameters, 3 Euler angles for each glycolate molecules, 4 isotropic temperature factors, one for each molecule and one for free atoms Co and Cl, 6 anisotropic thermal parameter β_{ij} for Eu atoms. Crystal data and structure refinement parameters are reported in Table 1.

Table 1. Crystal data and structure refinement parameters of the CoEu-based complex.

Compound	$EuCoCl(deg)_2$
Formula sum	$C_8O_6H_8Eu_1Co_1Cl_1$
Fw(g.mol^{-1})	454.56
System	Monoclinic
Space group	C 2/c
a (Å)	18.0507(1)
b (Å)	11.58354(6)
c (Å)	14.95352(7)
β(°)	121.9316(4)
V (Å^3)	2653.5(4)
Z	8
Dx (g.cm^{-3})	2.276
Wave length (Å)	0.66633
2θ range (deg)	3.1-36.0
N obs of points	16450
N_{ref}	1143
Rp	0.103
Rwp	0.134
R_{bragg}	0.060
R_F	0.071
N profile parameters	10
N intensity dependent parameters	36

The starting model given by FOX program converged very satisfactorily to R_{Bragg} = 6%. The relaxed geometrical parameters of deg_A and deg_B molecules and the atomic coordinates of the whole CoEu-based glycolate complex used in the Rietveld refinement are reported in the supporting information section (see Table S1 and Table S2, respectively, in the supporting information section). The high quality of the refinement is illustrated in the supporting information section through the perfect superposition of the experimental pattern with the calculated one (see Figure S2 in the supporting information section).

Note all the other patterns of produced complexes were indexed in the same structure. The refined lattice parameters and the unit cell volume V of all the produced powders (Table 2) agree very well with the lanthanide contraction. They decrease linearly when the Ln atomic number increases (Figure 2).

Table 2. List of refined lattice parameters of all the produced CoLn-based complexes.

Ln	Z	a(Å)	b(Å)	c(Å)	β(°)	V(Å^3)
Nd	60	18.132	11.692	15.241	122.46	2726.33
Sm	62	18.110	11.656	15.076	122.08	2695.71
Eu	63	18.093	11.611	14.991	121.95	2672.48
Gd	64	18.089	11.608	14.948	121.84	2666.59
Ho	67	18.063	11.536	14.693	121.43	2612.43

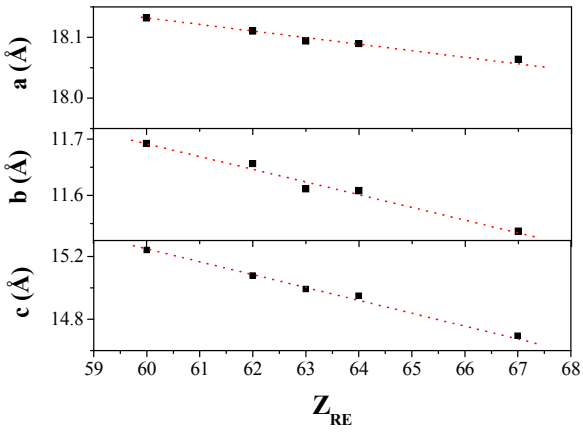

Figure 2. Variation of the refined lattice cell parameters of the produced CoLn-based complexes as a function of Ln atomic number.

Optical and X-ray Absorption measurements

The local structure was inferred first from the UV-visible diffuse reflectance spectra of the as-produced powders using a Perkin Elmer-Lambda 1050 spectrophotometer equipped with a PTFE-coated integration sphere. The spectra were analyzed with a special emphasis on the d-d transitions of $3d^7$ Co cations. Second, Extended

X-ray Absorption Fine Structure (EXAFS) spectroscopy was carried out. Data were specifically collected at the Eu L_3-edge at 300 K, using a transmission mode detection scheme with a Si (111) two-crystals monochromator on the SAMBA beamline of the SOLEIL storage ring at the French facility (Orne Les Merisiers). The sample was ground and homogeneously dispersed in cellulose pellets. EXAFS data were analyzed using the IFEFFIT software. [21] Typically, the pre-edge contribution was fitted by a linear curve and subtracted from the total absorption. Above the edge, the absorption coefficient μ(E) contains both the isolated atom contribution $\mu_0(E)$ and the structural contribution. $\mu_0(E)$ was computed as the smooth part of μ(E) after the edge, and then subtracted from μ(E) to deduce the relative variation of the absorption coefficient with respect to that of the free absorbing atom: $\chi(E) = (\mu(E)-\mu_0(E))/\mu_0(E)$. This interference function is reported as a function of the wave vector k and the Fourier transform (FT) of the $\chi(k).k^3$ product was calculated (the waiting factor k^3 was introduced to overcome the damping of the EXAFS oscillations at the large k values) and its Fourier transform (FT) was determined. The FT moduli are representative of the radial distribution function of back-scatterers around the absorbing atom. Both total EXAFS interference function and its FT moduli are plotted in the supporting information section (see Figure S3 in the supporting information section). Finally, least square modeling using single scattering Eu EXAFS simulation on the inverse Fourier transform of the first filtered peak corresponding to the first back-scatterer atom shells (see the windows function associated to the cut-off distances on both sides of the selected FT peak in Figure S3) was performed. The fitting procedure is based on the equation: [21]

$$k\ \chi(k) = \sum_i \frac{N_i}{R_i^2} \exp(-2k^2\sigma_i^2) \exp\left(-\frac{2R_i}{\lambda(k)}\right) \left| f_i(\pi,k) \right| \sin(2kR_i + \Phi_i(k))$$

where N_i is the number of back-scatterers "i" at a distance R_i from the central atom and σ_i the Gaussian Debye-Waller factor associated with R_i. The energy threshold, E_0, taken at the first inflexion of the absorption edge is corrected in the fitting procedure by the ΔE_0 parameter and finally the $|f_i(\pi,k)|$ and $\Phi_i(k)$ corresponding to the amplitude and phase shift functions, respectively, were calculated from FEFF7 program for each back-scatterers type shell, [22] using the structural data inferred from the crystallographic analysis. In practice, the very good agreement between the calculated interference function using previous equation and the experimental one allowed us to stop the recurrence process.

Magnetic properties

The thermal variation of the magnetic susceptibility, χ(T), of all the produced powders was collected on a Quantum Design SQUID-7T magnetometer at a dc magnetic field of 500 Oe, in the 2-300 K temperature range. The thermal variation of their magnetic heat capacity, $C_P(T)$, was also recorded on a Quantum Design PPMS-9T magnetometer, in the 2-150 K temperature range. Typically, a given mass (some mg) of the polycrystalline specimens was compacted into a sampling plastic tube to avoid grains displacement during the measurements and introduced in the magnetometers. Note, the magnetic responses were corrected from the diamagnetic blank data of the sample holder obtained separately, and the diamagnetic contribution of the samples themselves, estimated from Pascal's constants. The thermal variation of the real and imaginary parts of the ac magnetic susceptibility was also recorded at different frequencies from 1 to 1000 Hz, for a magnetic field of a magnitude of 3 Oe.

Results and discussion

Phase analysis

XRF analysis showed that the produced powders contain chloride, cobalt and Ln atoms in the 1:1:1 ratio. It also evidenced a high carbon and oxygen content, suggesting the formation of a metal-organic hybrid material. The recorded FTIR spectrum on the CoEu-based compound compared to that of free $degH_2$ permitted us to identify diethyleneglycol ($degH_2$) and/or diethyleneglycolate (deg) as the main organic constituent (Figure 3a) suggesting the formation of a heterometallic (Co and Eu) glycolate complex.

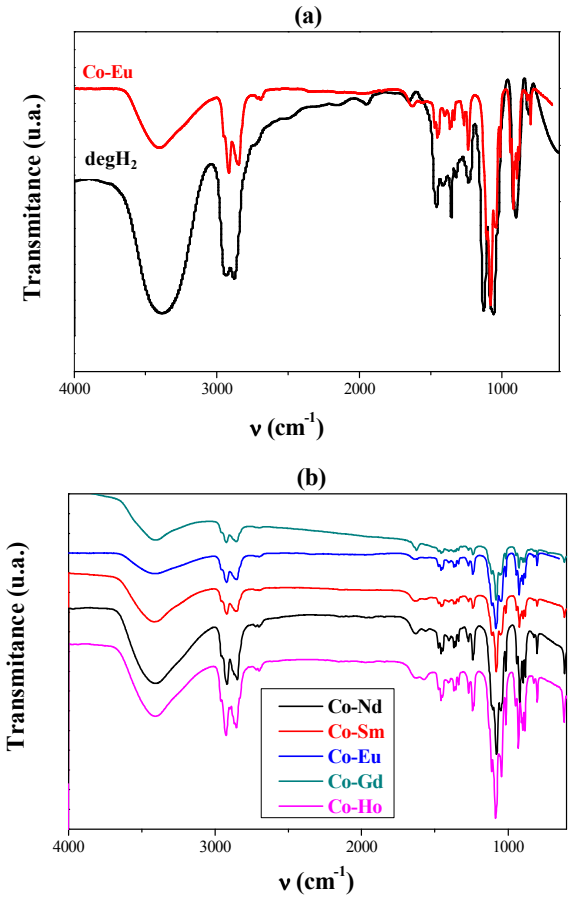

Figure 3. FTIR spectrum of the as-produced Co-Eu glycolate complex compared to that of free $degH_2$ (a) and to those of the other Co-Ln complexes (b).

Indeed, a broader band occurring at 3410 cm^{-1} was observed. It was

attributed to the stretching vibration of OH groups linked by hydrogen bonds from diethyleneglycol or water molecules. Strong absorptions were observed in the 2850–2950 cm^{-1} range, corresponding to ν_{as}(C-H) and ν_s(C–H) bands, and at 1050–1125 cm^{-1}, corresponding to $\rho(CH_2)$, ν(C–O) and ν(C–C) bands. [23] It is noteworthy that the bands in the 1300–1450 cm^{-1} range present in the $degH_2$ spectrum are no longer observed in the studied powder. This can be attributed to the absence of protons in the glycolate-like phase and thus the disappearance of the δ(C–OH) bands. The CH stretching vibration bands are split (2954, 2922, 2884 and 2854 cm^{-1}) in the glycolates with respect to free $degH_2$ (2962 and 2877 cm^{-1}). This is the result of a chelating coordination to the cations that lowers the symmetry of the ligand and increases the number of absorptions. [24]

Interestingly, the intrinsically weak basicity of the acetate counter-ion induces $degH_2$ deprotonation, at least once, and the formation of its alcoholate ions. This may be possible thanks to the reaction of acetate ions with water molecules, resulting from the dissolution of the hydrated metallic salts, producing hydroxide groups which in turn deprotonate, at least partially, the alcohol species:

$CH_3COO^- + H_2O = CH_3COOH + OH^-$

$OH^- + (HOC_2H_4)_2O = H_2O + HO(C_2H_4)O(C_2H_4)O^-$

Such mechanism was already proposed to explain the production of cobalt ethanediolate and propanediolate in 1,2-ethanediol and 1,2-propanediol, respectively, starting from hydrated cobalt(II) acetate salts. [16] The direct $degH_2$ deprotonation by acetate is also possible. Several examples were reported in the organometallic literature where just a weak base is needed to deprotonate alcohols, the reaction often being governed by the strength of the forming metal-ligand bonds. [25]

In our case, the formation of the heterometallic glycolate requires the presence of both chloride and acetate ions in the reaction medium. Indeed, starting from only acetate or only chloride metallic salts did not induce the precipitation of the purple solid phase. This suggested that chloride anions may exist as a counter ion with polycationic cluster with metals and glycolates or may enter in the coordination sphere of at least one metal cation to stabilize the final inorganic structure. All together, these results conduced us to propose $CoEuCl(deg)_x.nH_2O$ chemical composition for the produced powder, where deg corresponds to the deprotonated form of $degH_2$, x its stoichiometry coefficient and n the number of hydratation. Replacing Eu by another Ln cation leads to the same kind of compounds. Similar FTIR spectra are recorded whatever the nature of Ln cation (Figure 3b).

To determine the exact chemical composition of the studied glycolates, thermal analysis was performed for all the produced compounds. The air thermogramm of the representative CoEu-based complex is given in figure 4. A unique total weight loss of 40.4 wt.-% was observed around 300°C. It was associated to two exothermic heat flow peaks, corresponding to the complete decomposition of the complex and leading to the formation of $EuCoO_3$ oxide as confirmed by XRD analysis of the final product. The inferred molecular weight from this mass loss analysis is of 450 $g.mol^{-1}$ which is very close to that of $EuCoCl[(OC_2H_4)_2O]_2$ chemical formula in which two DEG molecules were deprotonated twice and where the electro-neutrality of the final product was respected, Co and Eu cations being at the oxidation state +2 and +3, respectively.

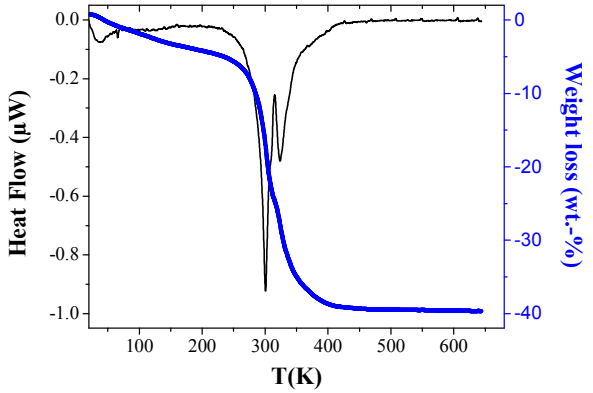

Figure 4. Air thermogram of the as-produced CoEu-based solid precipitate in polyol.

Note the compound is anhydrous and the total oxidation of $EuCoCl[(OC_2H_4)_2O]_2$ leads to a total organic weight loss of 43 wt.-%, very close to that measured by TGA.

Structural description

The local environment of metallic cations is shown in figure 5 and its general representation in figure 6 for CoEu-based complex. Co^{2+} cations, the center of the trigonal bi-pyramid, are fivefold coordinated with four Co-O distances ranging between 1.91 and 2.22 Å and one Co-Cl distance of 2.25 Å. Among the four O atoms, three belong to one deg_A and the last to one deg_B ligand. Eu^{3+} is seven fold coordinated by O atoms belonging to five distinct glycolate molecules. Three O atoms come from the same deg_B, two O-atoms come from two deg_A and two O-atoms come from two other distinct deg_B, to ensure the coordination with the other tetrameric subunits.

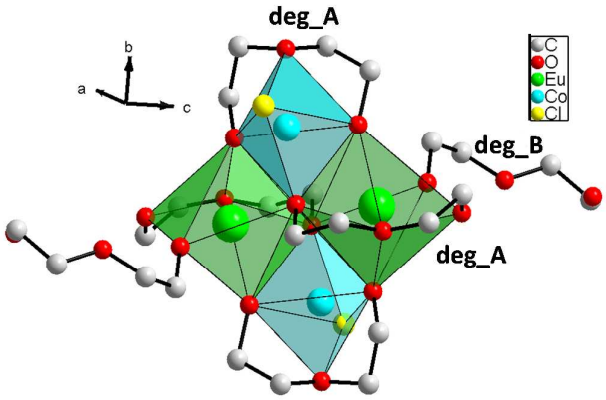

Figure 5. Structural details of the tetrameric $[(Eu_2Co_2)(deg)_4(Cl)_2]$ sub-unit constituting the CoEu-based glycolate complex.

The interatomic distances Eu-O range between 2.274 and 2.492 Å. Polyhedron around Eu atoms can be view as a mono capped trigonal antiprism. Bond valence calculations (Table 3) are in agreement with a trivalent europium and divalent cobalt. By connection of the preceding polyhedrons, tretrameric sub-units can be considered $[(Eu_2Co_2)(deg)_4(Cl)_2]$ for the description. Two mono capped trigonal antiprims

'EuO_7' related by the inversion center are linked by edges forming first the dimere unit 'Eu_2O_{12}'. Two trigonal bi-pyramids center by Co^{2+} and related by the same symmetry center complete the motif leading to the tetrameric sub unit where the two 'CoO_4Cl' polyhedra are isolated from each other by Ln atoms. Among the six glycolate molecules of the tetrameric sub unit, two deg_A and two deg_B molecules are tridentate and chelating and two others deg_B molecules bridge the adjacent tetramer along the c direction. Inside the tetrameric unit, the two Eu or the two Co atoms are related by a symmetry center. Eu-Eu and Co-Co distances are 3.965 and 5.444 Å respectively.

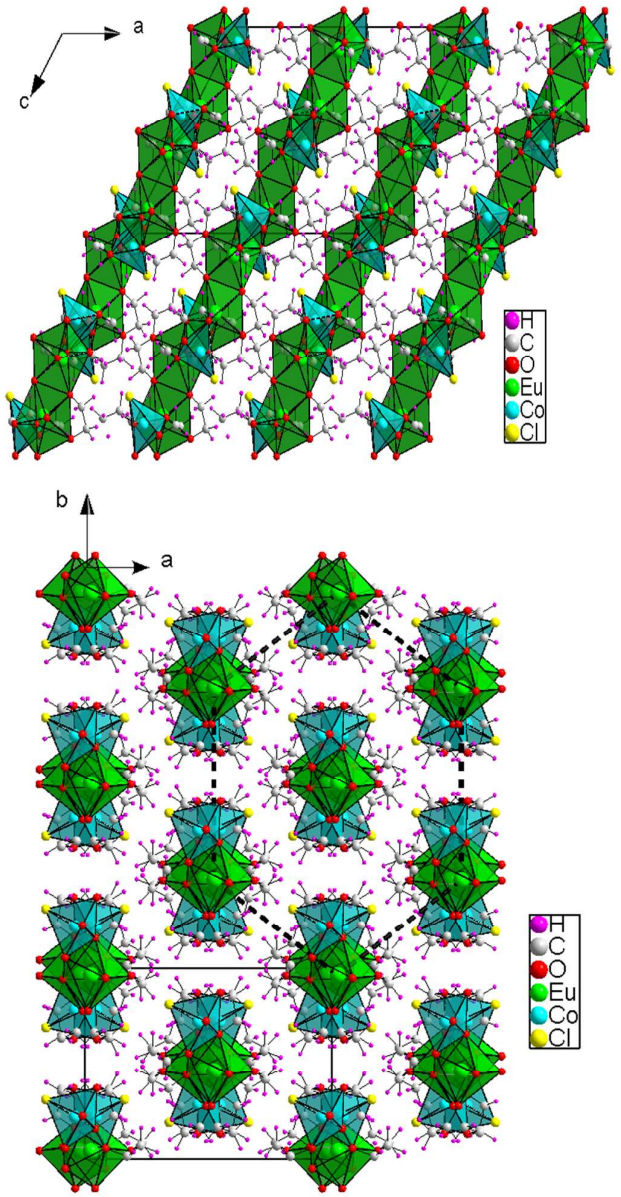

Figure 6. Projection along the b and c axes of the crystallographic lattice of CoEuCl(deg)$_2$ complex. Dashed line emphasis the pseudo hexagonal network arrangement of the 1D chains

Adjacent tetrameric units are generated by the c mirror perpendicular to b. In between adjacent tetramers, shorter Eu-Eu distance of 3.739 Å and longer Co-Co distance of 6.16 Å are observed. Connection of the infinite tetrameric chains is realized by Van der Waals interactions only. Indeed, all O atoms of the glycolate molecules participate to the coordination of both metallic elements. Thus, the shortest O-O interchain distance is of 5.04 Å, meaning impossibility for having hydrogen bonds where O-O between donor and acceptor is usually around 2.9 Å. Each chain is connected by van der Waals interaction to six other chains in a pseudo hexagonal network as shown in Figure 6.

Table 3. Selected inter-atomic distances (Å) in EuCoCl(deg)$_2$ complex.

Atom	O-Atom	Distance	Bond valence
Eu	A_3^{iii}	2.274(16)	0.583
	A_13^{ii}	2.2628(17)	0.602
	B_3^{i}	2.2743(14)	0.583
	B_3^{ii}	2.427(2)	0.386
	B_6^{ii}	2.4924(15)	0.324
	B_13^{ii}	2.4532(18)	0.360
	B_13^{iii}	2.452(2)	0.361
			Ox. State = 3.20
Co	A_3^{iv}	1.908(5)	0.558
	A_6^{iv}	2.228(3)	0.235
	A_13^{iv}	2.019(5)	0.413
	B_13^{iv}	2.050(4)	0.380
	Cl^{v}	2.250(6)	0.556
			Ox. State = 2.14
Co	Eu^{vi}	3.361(1) intra	
	Eu^{vii}	3.373(1) intra	
Eu	Eu^{viii}	3.965(1) intra	
Co	Co^{ix}	5.444(1) intra	
Co	Co	6.162(1) inter	
Eu	Eu	3.739(1) inter	

Symmetry codes: (i) 0.5+x, -0.5+y, z; (ii) 1.5-x, -0.5+y, 0.5-z; (iii) 0.5+x, 0.5-y, -0.5+z; (iv) -0.5+x, 0.5-y, -0.5+z; (v) x, -y, -0.5+z, (vi) -1+x, y, z; (vii) 1-x, -y, -z; (viii) 2-x, -y, -z; (ix) -x, -y, -z.

Optical diffused reflectance and X-ray absorption spectroscopies results

The recorded UV-visible diffused reflectance spectrum of the produced CoEuCl(deg)$_2$ complex exhibited more than four spin allowed absorptions (see figure 7): two well resolved and intense bands at 274 and 560 nm, a spilt one at 841 and 994 nm and a broad and degenerate one with three maxima at 1812, 2006 and 2200 nm. There are much more absorption bands than those expected from the energy level diagram of a d^7 ion in an octahedral, [26] tetrahedral, 26 neither square pyramidal [27] crystal field. A rapid overview of the relevant literature suggests that the obtained optical data agree with those of high-spin five-coordinated Co^{2+} ion in a more or less deformed trigonal bipyramidal crystal field. The energy level diagram of such cation symmetry involves six spin allowed d-d transitions: [28]
$^4A_2'(^4F) \rightarrow {}^4A_1''(^4F)$; $^4A_2'(^4F) \rightarrow {}^4A_2''(^4F)$; $^4A_2'(^4F) \rightarrow {}^4E''(^4F)$; $^4A_2''(^4F) \rightarrow {}^4E'(^4F)$; $^4A_2'(^4F) \rightarrow {}^4A_2'(^4P)$ and $^4A_2'(^4F) \rightarrow {}^4E''(^4P)$, whose energy positions appear to be close to those measured. [29]

Interestingly, all synthesized samples CoLn glycolates present the same d-d broader bands with additional contributions related to the spectroscopic atomic absorption of their constituting Ln cations, meaning the same environment for cobalt cations in all the studied sample series (Figure 7).

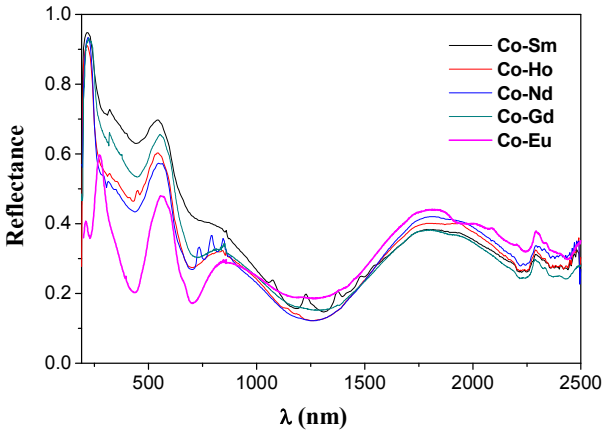

Figure 7. UV-visible diffused reflectance spectra of $CoLnCl(deg)_2$ complexes (Ln = Nd, Sm, Eu, Gd, Ho).

To confirm the local structure provided from XRD analysis around Ln cations, L_3(Eu) EXAFS spectrum of the representative $CoEuCl(deg)_2$ complex of the studied sample series was collected and analyzed according the procedure detailed in the experimental section. The peaks in the FT moduli of the total EXAFS function weighted by k^3, reported in Figure S3, correspond to apparent interatomic distances, uncorrected for central and backscattering electron phase shifts. The main peak, comprised between R = 1.2 and 3.6 Å, and associated to the shells of nearest (nn) and next to nearest (nnn) atoms of Eu is clearly identified. According the crystallographic data, the nn shell consists of seven oxygen atoms of DEG molecules directly attached to Eu cation at a distance ranging between 2.25 and 2.50 Å and forming its first coordination sphere (main contribution) while the nnn one consists of four carbon atom from the same DEG molecules a distance ranging between 3.15 and 3.35 Å and two cobalt atoms of the same tetrameric unit at a distance of about 3.35 Å (minor contribution).

By inverse Fourier transform of this peak, the contribution to the total EXAFS signal χ(k) of these nn and nnn shells is reported in Figures 8a (blue line) and its fit (red line) according to the equation given in the experiment section. The Fourier transform of the filtred EXAFS signal (blue line) was also determined and superposed to the calculated peaks for both nn and nnn shells.

The best fit was obtained by considering two distinct nn Eu-O shells, one at a shorter Eu-O distance, ~2.25 Å (the green line in Figure 8b), and one at a longer distance, 2.45 Å (the purple line in Figure 8b) and three distinct nnn shell, a Eu-C one at about 3.25 Å (the orange line in Figure 8b), a Eu-Co one at 3.35 Å (the brown line in Figure 8b) and a Eu-O one at about 3.55 Å (the pink line in Figure 8b). The refined interatomic distances, Debye-Waller factor and number of back-scatterers for all these shells are summarized in Table 4, agreeing very well with Rietveld results.

Table 4. EXAFS refinement results at L_3(Eu) edge. N measures the number of back-scatterers at a distance R from the central atom, σ^2 the Gaussian Debye-Waller factor associated with R. Note that the energy threshold, E_0, taken at the first inflexion of the L_3(Eu) absorption edge is corrected in the fitting procedure by the ΔE_0 parameter.

pair	N	R Å	ΔE_0 eV	σ^2 Å^2
Eu-O1	3	2.26 ± 0.02	0.071 ± 0.010	0.0062 ± 0.0016
Eu-O2	4	2.45 ± 0.02	0.054 ± 0.011	0.0068 ± 0.0018
Eu-C	4	3.30 ± 0.02	0.244 ± 0.016	0.0049 ± 0.0016
Eu-Co	2	3.36 ± 0.02	0.146 ± 0.013	0.0179 ± 0.0024
Eu-O3	1	3.55 ± 0.02	0.082 ± 0.043	0.0191 ± 0.0099

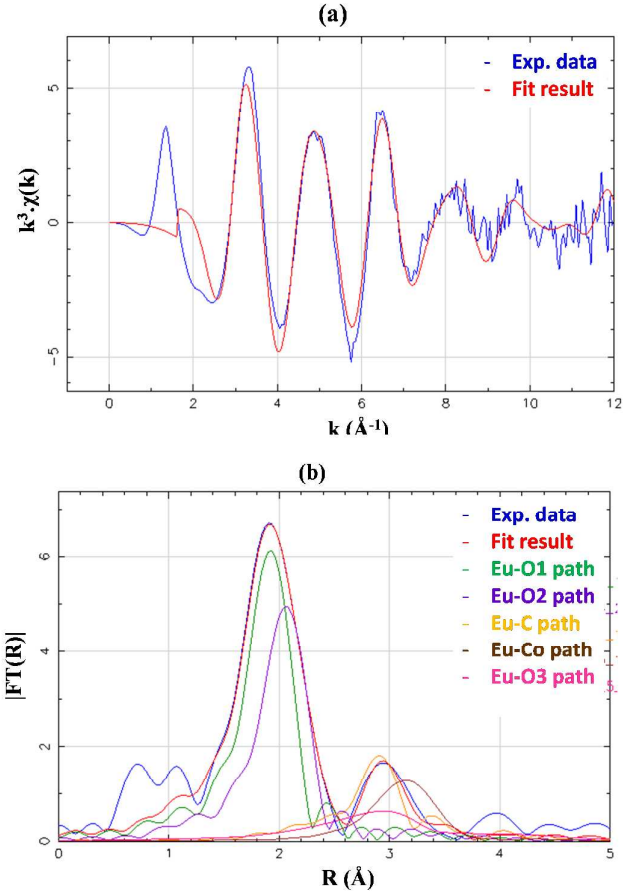

Figure 8. Filtered EXAFS interference function as a function of the wave vector k of the photoelectron (blue line) superposed to the calculated contribution of the nn and nnn shells around Eu to the total EXAFS signal (red line) (a). The Fourier transform of the filtred EXAFS signal (blue line) superposed to the calculated contribution of both nn (Eu-O1 in green and Eu-O2 in purple) and nnn (Eu-C in orange, Eu-Co in brown and Eu-O3 in pink) shells (b)

Magnetic properties

The thermal dependence of the static molar susceptibility χ has been recorded for all produced complexes (Figure 9).

As a first lecture, the monotonous variation of $\chi(T)$ at low magnetic field (500 Oe) and the linear variation of $\chi^{-1}(T)$ at high temperature suggest that $CoLnCl(deg)_2$ complexes are paramagnetic in this temperature range. The linear fit of $\chi^{-1}(T)$ by the Curie-Weiss law in the 100-300 K range allows us to determine the Curie constant, C and the Weiss temperature θ_p, which are summarized in Table 5 and compared to theoretical values, calculated per mole of complex, considering Ln^{3+} and Co^{2+} cations in their ground state and neglecting the orbital contribution of the latter (spin only theory):

$$C_{the} = \frac{N\beta^2}{3k_B}\left[g_e^2 S_{Co}(S_{Co}+1) + g_J^2 J_{Ln}(J_{Ln}+1)\right]$$

$$g_J = 1 + \frac{J_{Ln}(J_{Ln}+1) + S_{Ln}(S_{Ln}+1) - L_{Ln}(L_{Ln}+1)}{2J_{Ln}(J_{Ln}+1)}$$

The measured Curie constants are not exactly equal to those calculated, pointing out the fact the cobalt orbital contribution must not be neglected in the total magnetic response. In the case of CoSm and CoEu systems, because the first excited, J=7/2 and J=1, Sm^{3+} and Eu^{3+} multiplets are relatively close in energy to the fundamental J=5/2 and J=0 multiplets, respectively, [30] it would be necessary to account not only the fundamental state, but also these excited multiplets in their related magnetic contribution. The mixing of these higher multiplets into the fundamental leads to a decrease and an increase of the magnetic moment of Sm^{3+} and Eu^{3+} cations, respectively. [31] In the paramagnetic range the consequence of this mixing is a magnetic susceptibility, which is the sum of a Curie-type term, inversely proportional to the temperature, and a Van Vleck-type term, independent of the temperature, [30,31] underlining the limit of our model at least for these two compounds and explaining the observed huge differences between C_{exp} and C_{the} for them (see table 3). Anyway, the obtained C_{exp} values serve as numbers for comparison into the studied sample series. It globally increases when the number of 4f electron increases.

Table 5. List of the measured Curie constant, C_{exp} and Weiss temperature θ_p for all the produced complexes. The calculated C_{the} values assuming Curie law for a high spin Co^{2+} (spin only) and Ln^{3+} cations are given for comparison

Co-*Ln*	*Ln* ground state	C_{exp} (cm^3 K mol^{-1})	C_{the} (cm^3 K mol^{-1})	θ_p (K)
Co-Nd	$^4I_{9/2}$	4.86	3.511	-20
Co-Sm	$^6H_{5/2}$	3.15	4.336	-53
Co-Eu	$^7F_0$	4.16	1.876	-64
Co-Gd	$^8S_{7/2}$	11.35	9.750	-40
Co-Ho	$^5I_8$	15.77	15.937	-51

The θ_p value is negative and weak giving evidence that antiferromagnetic interactions exist at short-range between the paramagnetic cations. Considering the structure of the produced complexes, the large separation between consecutive Co^{2+} and Ln^{3+} cations inside the lattice makes Co-Co and Ln-Ln superexchange interactions negligible. Only weak exchange interactions between the 3d Co^{2+} and 4f Ln^{3+} orbitals through the 2p μ^2-oxygen atom orbitals of bridging deg ligands inside a tetramer are noted, leading to small θ_p values.

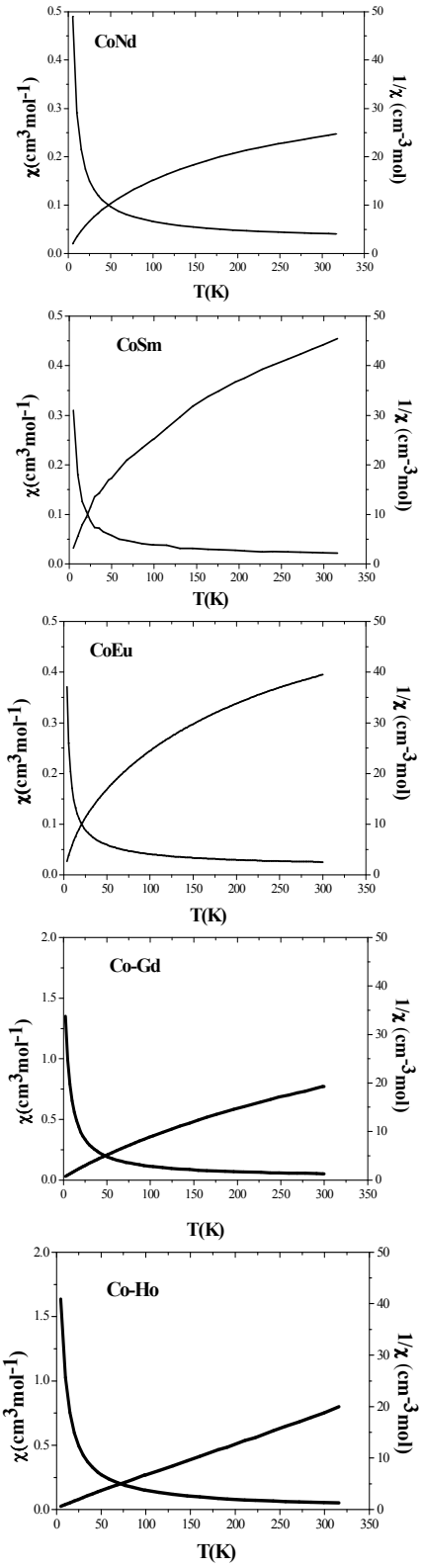

Figure 9: Temperature dependence of the magnetic molar dc-susceptibility χ (left axis) and its reciprocal function χ^{-1} (right axis) measured on the as-produced $CoLnCl(deg)_2$ complexes (Ln = Nd, Sm, Eu, Gd, Ho), under an applied field of 500 Oe.

These interactions may explain the observed deviation from the Curie law at low temperature (below 50 K) on the collected data, even if the establishment of a long range antiferromagnetic order is not evidenced down to 2 K. The presence of spin–orbit coupling effects in these lanthanide derivatives makes the fitting of the data to obtain Co^{2+}-Ln^{3+} exchange parameters far from straightforward

The experimental magnetometry data were also plotted as χ.T versus T for all the CoLn compounds (see Figure S4 in the supporting information section). The obtained curves are typical of weakly antiferomagnetically interacting spin systems: χ.T decreases continuously when T decreases. Varying the magnitude of the applied field below and above 500 Oe (typically at H = 50 and 1000 Oe), the same shape of the curve is observed (not shown).

Besides, the thermal variation of the heat capacity of these compounds do not feature any anomalies below 150 K and do not undergo any phase transformation. No obvious λ peak is found in the measured temperature range, which is a clear evidence for the absence of 3D magnetic ordering in agreement with their pseudo 1D structure. To illustrate that the recorded C_p versus T curve for CoEu system is given in Figure 10.

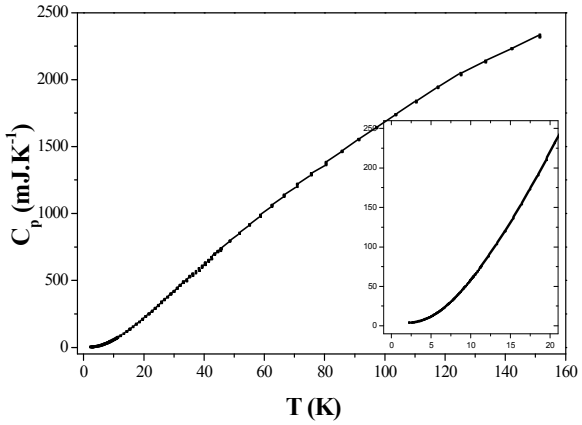

Figure 10. Thermal variation of the magnetic heat capacity C_p of $CoEuCl(deg)_2$. A zoom of the low temperature range is given in the inset.

This feature was also confirmed by dynamic ac-magnetization measurements. The thermal variation of the out-of-plane ac-susceptibility component (χ'') of two representative compounds, namely CoEu and CoGd ones, plotted in figure S5, show unambiguously a χ'' equal to zero in all the explored temperature and frequency ranges.

This feature is usually consistent with non-magnetically long-range ordered systems.

Regarding the initial objective of the work

Based on all these structural information, one may suppose that the produced glycolates when redispersed in a polyol and heated under optimized conditions (temperature, NaOH or KOH concentration, reacting time, inert atmosphere…) should provide the liberation of molecular species whom composition must be very close to the previously described tetrameric sub-unit, in which both Co^{2+} and Ln^{3+} cations are simultaneously coordinated to dielthyleneglycolate ligands. The proximity of the two cations should favor their simultaneous reduction. Assays using these compounds as starting materials for the production of their related alloyed nanoparticles in polyol are in progress. They will be described in further works.

Conclusions

$CoLnCl[(O(C_2H_4O)_2)_2]$ (Ln = Nd, Sm, Eu, Gd and Ho) chloro-glycolate poynuclear hybrid were produced by reaction of cobalt acetate and Ln chloride salts in boiling diethyleneglycol. Interestingly, non-conventional five and seven coordination spheres were evidenced around cobalt (II) and Lanthanide (III), respectively. These cations were coordinated by O-atoms of deprotonated diethyleneglycol molecules. The structure consist of 1D magnetic chains running along c direction and packed together in a pseudo hexagonal framework maintained by Van der Waals interactions (there are no direct magnetic pathway between the chains). The CoLn compounds exhibit weak Co-Ln antiferromagnetic interactions within the tetrameric clusters. These materials could be used as starting materials for TM-Ln nanoparticles production in polyol.

Acknowledgements

The authors acknowledge SOLEIL for provision of synchrotron radiation facilities. They particularly would like to thank V. Briois (Samba beamline) and E. Elkaim (Crystal beamline) for their assistance during synchrotron measurements.

Notes and references

Abbreviations

$degH_2$, dethyleneglycol; deg, diethyleneglycolate; XRD, X-ray diffraction; XRPD, High resolution X-ray Diffraction, XRF, X-ray Fluorescence spectrometry.

References

1 K. J. Strnat, D. Li and H. F. Mildrum, *J. Appl. Phys.* 1984, **55**, 2100.
2 N. Tang, Z. Chn, Y. Zhang, G. C. Hadjipanayis and F. J. Yang, *J. Magn. Magn. Mater.* 2000, **219**, 173.
3 Z. D. Zhang, W. Liu, J. P. Liu, and D. J. J. Sellmyer, *J. Phys. D: Appl. Phys.* 2000, **33**, R217C.
4 M. Foldeaki, A. Giguère, B. R. Gopal, R. Chahine, T. K. Bose, X. Y. Liu and J. A. Barclay, *J. Magn. Magn. Mater*. 1997, **174**, 295.
5 C. D. Stanciu, A. V. Kimel, F. Hansteen, A. Tsukamoto, A. Itoh, A. Kirilyuk and T. Rasing, *Phys. Rev. B* 2006, **73**, 220402.
6 T. W. McDaniel, *J. Phys.: Condens. Matter* 2005, **17**, R315.
7 V. M. Chakka, B. Altuncevahir, Z. Q. Jin, Y. Li and J. P. Liu, *Appl. Phys.* 2006, **99**, 08E912 ; A. Bajorek, P. Skornia, K. Prusik, M. Wojtyniak and G. Chelkowska, *Mater. Characterization* 2015, **101**, 58.
8 B. Balasubramanian, R. Skomski, X. Li, S. R. Valloppilly, J. E. Shield, G. C. Hadjipanayis and D. J. Sellmyer, *Nano Lett.* 2011, **11**, 1747.

9 Y. Hou, Z. Xu, S. Peng, C. Rong, J. P. Liu and S. Sun, *Adv. Mater.* 2007, **19**, 3349.
10 S. J. Shin, Y. H. Kim, H. G. Cha, C. W. Kim and Y. S. Kang, *Mol. Cryst. Liq. Cryst.* 2007, **464**, 39/621.
11 M. Figlarz, F. Fiévet and J. P. Lagier, Europe n°0113281, USA n°4539041, Finlande n°74416, Japon n°04024402, 1982.
12 F. Bonet, V. Delmas, S. Grugeon, R. Herrera-Urbina, P. Y. Silvert and K. Tekaia-Elhsissen, *Nanostruct. Mater.* 1999, **11**, 1277 ; N. Chakroune, G. Viau, C. Ricolleau, F. Fiévet-Vincent and F. Fiévet, *J. Mater. Chem*. 2003, **13**, 312 ; F. Fiévet, F. Fiévet-Vincent, J. P. Lagier, B. Dumont and M. Figlarz, *J. Mater. Chem.* 1993, **3**, 627 ; B. Jeyadevan, A. Hobo, K. Urakawa, C. N. Chinnasamy, K. Shinoda and K. Tohji, *J. Appl. Phys,* 2003, **93**, 7574 ; Y. Soumare, C. Garcia, T. Maurer, G. Chaboussant, F. Ott, F. Fiévet, J. Y. Piquemal and G. Viau, G. *Adv. Func. Mater*. 2009, **19**, 1971.
13 T. Matsushita, T. Iwamoto, M. Inokuchi and N. Toshima, *Nanotechnology* 2010, **21**, 095603.
14 C. N. Chinnasamy, J. Y. Huang, L. H. Lewis, B. Latha, C. Vittoria and V. G. Harris, *Appl. Phys. Lett*. 2008, **93**, 032505.
15 V. G. Harris, Y. Chen, A. Yang, S. Yoon, Z. Chen, A. L. Geiler, J. Gao,C. N. Chinnasamy, L. H. Lewis, C. Vittoria, E. E. Carpenter, K. J. Carroll, R. Goswami, M. A. Willard, L. Kurihara, M. Gjoka and O. Kalogirou, *J. Phys. D: Appl. Phys.* 2010, **43**, 16500.
16 N. Chakroune, G. Viau, S. Ammar, N. Jouini, P. Gredin, M. J. Vaulay and F. Fiévet, *New J. Chem*. 2005, **29**, 355 ; D. Larcher, G. Sudant, R. Patrice and J. M. Tarascon, *Chem. Mater*. 2003, **15**, 3543.
17 F. Fiévet, Synthesis, characterization and mechanism growth, in Fine Particles, edited by T. Sugimoto, Marcel Dekker, Inc, Tokyo, 2000.
18 K. J. Carroll, J. U. Reveless, M. D. Shultz, S. N. Khanna and E. E. Carpenter, *J. Phys. Chem. C* 2011, **115**, 2656 ; R. J. Joseyphus, T. Matsumoto, H. Takahashi, D. Kodama, K. Tohji, and B. Jeyadevan, *J. Solid State Chem.* 2007, **180**, 3008 ; H. Yoon, A. Xu, G. E. Sterbinsky, D. A. Arena, Z. Wang, P. W. Stephens, Y. S. Meng and K. Carroll, *J. Phys. Chem. Chem. Phys.* 2015, **17**, 1070.
19 V. Favre-Nicolin and R. Černý, *Appl. Crys*. 2002, **35**, 734.
20 T. Roisnel and J. Rodriguez-Carvajal, *Mater. Sci. Forum*. 2001, **118**, 378 ; J. Rodriguez-Carvajal, *Physica B: Condens. Matter.* 1993, **192**, 55.
21 M. Newville, *J. Synchrotron Rad*. 2001, **8**, 322.
22 J. Mustre de Leon, J. J. Rehr, S. I. Zabinsky and R. C. Albers, *Phys. Rev. B.* 1991, **44**, 4146.
23 D. Knetsch and W. L. Groeneveld, *Inorg. Chim. Acta*. 1973, **7**, 81.
24 K. Tekaia-Elhsissen, A. Delahaye-Vidal, G. Nowogrocki, M. C. Figlarz, G. Nowogrocki and M. Figlarz, *CR. Acad. Sci., Ser. II: Mec. Phys. Chem. Sci. Terre Univers.* 1989, **309**, 349.
25 B. F. Abrahmas, A. H. Hudson and R. Robson, *Chem. Euro. J.* 2006, **12**, 7095 ; M. S. Sigman, R. David and D. R. Jensen, *Acc. Chem. Res.* 2006, **39**, 221 ; G. J. Ten, I. W. Brink, W. W. Arends, M. Hoogenraad, G. Verspui, and R. A. Sheldon, *Adv. Synth. Catal.* 2003, **345**, 1341 ; J. L. Durndell, A. F. Lee, D. S. Bailie and M. J. Muldoon in *Transition Metal Catalysis in Aerobic Alcohol Oxidation*, F. Cardona and C. Parmeggiani Eds, RSC Green Chemistry, 2014, **chap. 4**, 121.
26 A. B. P. Lever, *Inorganic Electronic Spectroscopy*, Elsevier, 2nd Ed, Amsterdam, 1984 ; M. Kurmoo, *J. Mater. Chem.* 1999, **9**, 2595 ; Y. Brik, M. Kacimi, M. Ziyad and F. Bozon-Verduraz, *J. Catalysis* 2001, **202**, 118 ; L. Poul, N. Jouini and F. Fiévet, *Chem. Mater*. 2000, **12**, 3123.
27 J. Kansikas, M. Leskela, G. Kenessey, T. Wadsten and G. Liptay, *Chem. Scandinavic.* 1996, **50**, 267 ; E. W. L. Darby and L. M. Vallarino, *Inorg. Chim. Act.* 1981, **48**, 215 . M. Ciampolini, *Struct. Bonding*. 1969, **6**, 52.
28 M. E. Foglio and G. E. Barberis, *Brazilian J. Phys.* 2006, **36**, 40.
29 T. J. Hubin, N. W. Alcock, H. J. Clase, L. L. Seib and D. H. Busch, *Inorg. Chim. Acta.* 2002, **337**, 91 ; M. Ciampolini and N. Nardi, *Inorg. Chem*. 1966, **5**, 41 ; V. L. Goedken, J. V. Quagliano and L. M. Vallarino, *Inorg. Chem*. 1969, **11**, 2331 ; L. Sacconi and I. Bertini, J. Am. Chem. Soc. 1966, **88**, 5180 ; L. Banci, A. Bencini C. Benelli, D. Gatteschi and C. Zanchini, *Struct. Bonding*. 1982, **52**, 37.
30 D. D. Pollock, *Physical Properties of Materials for Engineers*, CRC Press, Florida, 2nd edition, 1993 ; b) C. Opagiste, C. Barbier, R. Heattel and R. M. Galéra, *J. Magn. Magn. Mater*. 2015, **378**, 402 ; R. C. Layland, S. L. Kirkland and H. C. Zur Loye, *J. Solid State Chem.* 1998, **139**, 79.
31 K. H. J. Buschow, A. M. van Diepen and H. W. de Wijn, *Phys. Rev. B* 1973, **8**, 5134 ; A. Frank, *Phys. Rev*. 1932, **39**, 119.